Combining tensile tests and nanoindentation to explore the strengthening of high and medium entropy alloys

M. Laurent-Brocq, L. Perrière, R. Pirès, G. Bracq, T. Rieger, Y. Danard, I. Guillot

Version of Record: https://www.sciencedirect.com/science/article/pii/S2589152919302005
Manuscript_217184dd1bb545cf3a67408ae2d1abad

Combining tensile tests and nanoindentation to explore the strengthening of high and medium entropy alloys

M. Laurent-Brocq[1,*], L. Perrière[1], R. Pirès[1], G. Bracq, T. Rieger[1], Y. Danard[2], I. Guillot[1]

[1] ICMPE, UPEC-CNRS, 2 rue Henri Dunant, 94320, Thiais, France

[2] PSL Research University, ChimieParisTech - CNRS, Institut de Recherche de Chimie Paris, 75005, Paris, France

Corresponding author

First name: Mathilde ; Family name: Laurent-Brocq
E-mail: laurent-brocq@icmpe.cnrs.fr
Phone number : +33 (0)1 56 70 30 65
Postal adress : 2-8, rue Henri Dunant (bât D) F-94320 Thiais, France

Keywords

High entropy alloys; tensile test ; nanoindentation ; solid solution strengthening ; recrystallization

Abstract

Single-phase multi-component alloys exist for a very wide range of composition, which is still mostly unexplored. To determine the mechanical properties of one new medium entropy alloy (MEA) and to assess the potential of an accelerated testing strategy, the compositions CoCrFeMnNi, $(CoCrFeMn)_{40}Ni_{60}$ and $(CoCrFeMn)_8Ni_{92}$ were studied. They were processed in homogenized and recrystallized states, characterized by scanning electron microscopy coupled with electron backscattered diffraction and mechanically tested by tensile tests and nanoindentation. It was shown that the $(CoCrFeMn)_{40}Ni_{60}$ MEA exhibits as high tensile properties as the CoCrFeMnNi high entropy alloy. Not only the mechanical strength but also the ductility are the same in both alloys. Moreover, the uncertainty when comparing nanoindentation on homogenized samples with tensile yield strength was quantified. Knowing that, nanoindentation on homogenized HEA was identified as a powerful tool for fast exploring of chemical compositions and pre-selection of the most promising ones.

1. Introduction

High entropy alloys (HEA) are a new family of alloys which were discovered in 2004 [1, 2]. They are multi-component alloys, in which all elements are very concentrated (i.e.: there is no main nor minor elements) [3-6]. They can be either single-phase or multi-phase. At first, the focus was on single-phase HEA. Thus, the multi-phase HEA are sometimes also called second generation HEA or compositionally complex alloys [7]. This study will focus on single-phase HEA. The quinary equimolar CoCrFeMnNi, which is often named the Cantor alloy and which is composed of a unique face centered cubic solid solution [8], was one of the first discovered HEA [2]. It was proven to exhibit a high yield strength thanks to solid solution strengthening but also high strain hardening, ductility and toughness [9-11]. Since then, it was discovered that an extremely wide number of compositions, equimolar or not, can form a single-phase HEA [12], including within the Co-Cr-Fe-Mn-Ni system [13]. Several compositions were processed and mechanically tested. Some exhibit better mechanical properties compared to the Cantor alloy, like CoCrNi [14, 15], or equivalent ones, like $Cr_{18}Ni_{14}Fe_{40}Mn_{28}$ [16] while others may have lower ones, such as $Co_6Cr_2Fe_{26}Mn_{38}Ni_{28}$ [17] or CoFeMnNi [18]. Those results provide a glimpse of a possible further improvement of HEA mechanical properties.

However, it is also obvious that, to take advantage of the wide composition space and to fully optimize mechanical properties of single-phase HEA, accelerated mechanical testing tools are required [3, 7]. In that perspective, nanoindentation has been used to locally measure the hardness on compositionally graded HEA [19, 20]. Nanoindentation is also well-suited for small size and unrecrystallized samples, which can be easily and rapidly prepared. With this approach, the hardness of 10 compositions from the Ni isopleth (i.e. : $(CoCrFeMn)_{100-x}Ni_x$ with x varying from 0 to 92 % at.) was systematically measured by nanoindentation [21]. The hardness of the composition $(CoCrFeMn)_{40}Ni_{60}$ was highlighted to be the highest. Since Ni is the main element in this composition, it is more appropriate to qualify it as a medium entropy alloy (MEA) than as a HEA [3]. However, the hardness which is measured by nanoindentation does not completely describe the mechanical properties and, most of the time, it is only qualitatively compared to the intrinsic mechanical properties [20, 22, 23]. Consequently, the first objective of this study is to measure the mechanical properties of this new promising MEA by tensile testing for the first time. More specifically, it is intended to confirm the high solid solution strengthening (SSS) and to assess the ductility. The second objective is to quantitatively compare nanoindentation and tensile testing in order to establish the potential and the limits of nanoindentation for accelerated mechanical testing of HEA.

To do so, three compositions were selected: (i) the CoCrFeMnNi Cantor alloy, which is the reference HEA, (ii) the new promising $(CoCrFeMn)_{40}Ni_{60}$ MEA and (iii) $(CoCrFeMn)_2Ni_{92}$ which is a conventional diluted solid

solution. Those three compositions were processed, their microstructure was characterized and finally they were mechanically tested by tensile tests and by nanoindentation.

2. Methods

Ingots with the composition $(CoCrFeMn)_{(100-x)}Ni_x$ with x=20, 60 and 92 at. % were prepared by melting Co, Cr, Fe, Mn and Ni metals (with a purity exceeding 99.95 wt. %) by high frequency electromagnetic induction under an He atmosphere. Then gravity casting was performed to shape the ingots into rod with a diameter of 13 mm and a length of around 8 cm. Alloy preparation is detailed in [13]. Afterwards, three different sets of thermomechanical processing were performed for each sample. For the first set, a slice with a thickness of 2-3 mm was cut from the as-cast rod, which presents a dendritic microstructure [8]. Afterward this slice was wrapped into a tantalum sheet and homogenized at 1100°C during 13 h, under an He atmosphere. For the second set, the entire as-cast rod was homogenized with the previously exposed conditions. Subsequently, it was cold-rolled with a thickness reduction of 85-90 % to obtain a sheet with a thickness of 1.5 mm. Finally, a recrystallization annealing was performed under He atmosphere. Samples were introduced into the hot furnace, annealed and quickly cooled down, still maintained in the He atmosphere. In order to obtain a similar average grain size of around 15 µm, the temperature and duration of the recrystallization annealing were 900°C during 1h, 800°C during 2h and 800°C during 8h respectively for CoCrFeMnNi, $(CoCrFeMn)_{40}Ni_{60}$ and $(CoCrFeMn)_8Ni_{92}$. Those conditions were determined from previous study on the CoCrFeMnNi [9, 11, 24] and from preliminary tests. For the third set, the as-cast rod was cold rolled with a thickness reduction of 30 %, to obtain a parallelepiped with a width of around 9 mm. Afterwards, a slice of this parallelepiped with a thickness of 2-3 mm was annealed at 1250°C during 3 h under an Ar atmosphere and quickly cooled down to keep the high temperature stable phase. It is underlined that, because of the high temperature of the recrystallization annealing, an homogeneization treatment was unnecessary. Samples for microstructural and mechanical characterization were prepared by mechanical grinding using 1200 to 4000 grit SiC papers followed by a final polishing step using a vibratory table and a 0.04 µm colloidal silica for a minimum duration of 15 h.

Samples are named Nix-A where x is the atomic percent of Ni and where A describes the thermomechanical processing. A is either « homog » for the only homogenized samples (i.e. : first set), or « rec1 » for the samples which are recrystallized at intermediate temperatures, in order to obtain grain size around 15 µm (i.e. : second set) or « rec2 » for the samples which are recrystallized at high temperature in order to form large grains (i.e.: third set). All samples are listed in Table 1.

The microstructural characterization was performed with a Merlin Zeiss Field Emission Scanning Electron Microscope (FE-SEM) coupled with an Energy Dispersive X-ray Spectrometer (EDS) and an Electron BackScattered Diffraction detector (EBSD) from Oxford Instruments. Both detectors are driven by AZtec operating system. EDS mappings were performed to check the chemical spatial homogeneity and to measure the average composition (Table A1). The difference with the nominal composition is lower than 0.5 at. % for Co, Cr, Fe and Mn and lower than 1 at. % for Ni. To determine the grain size, the average diameter was calculated on EBSD mapping for the Nix-rec1 samples. Σ3 boundaries were not considered. The circular intercept method [25] was applied on SEM images for Nix-rec2 samples. In both cases, the given uncertainties correspond to the 95 % confidence interval. For Nix-homog samples, due to the irregular shape and very dispersed size of the unrecrystallized grains, only an approximate minimum grain dimension is given.

Mechanical tensile testing was performed for Nix-rec1. Rectangular dog-bone shaped tensile specimen with a gauge length of 30 mm and a gauge width of 6 mm were machined in the recrystallized sheets with a thickness of 1.5 mm by electrical discharge machining. Thus, the cross section of tensile specimen was containing more than 60 000 grains. Tensile tests were performed at room temperature and at an

engineering strain rate of 10^{-3} s^{-1} in a Criterion 43 MTS machine with a maximum force of 30 kN. The engineering strain was measured by an extensometer whose length was 25 mm. Three to four specimens were tested for each Nix-rec1 sample. The yield strength was determined at 0.2 % of plastic deformation. The uncertainties for the mechanical properties correspond to the standard deviation on the specimens of a given sample.

Finally, Nix-homog and Nix-rec2 samples were mechanically characterized by nanoindentation using a TI950 Hysitron indenter, which was equipped with a Berkovich diamond tip. The quality of the surface was checked on surfaces of 10*10 µm² by Scanning Probe Microscopy (SPM) [26], which consists in scanning the sample surface with the nanoindenter tip. Each indentation was performed with a constant strain rate loading of $\dot{h}/_{h} = 0.05\ s^{-1}$, where h is the indentation depth. The load was increased up to 12 mN, maintained during 5 s and unloaded for 5 s at a constant loading rate. The maximum indent depth was around 400 nm, depending on the composition. The continuous stiffness measurement (CSM) was set up at a frequency of 200 Hz, with an amplitude between 1 and 2 nm. Ten positions were randomly chosen on a sample and at each position, a group of ten indents, which were spaced from each other by 10 µm, was performed (Fig. 4a, b and c). In total, one hundred indents were performed on each sample (Fig. A2). Continuous stiffness measurement was used to calculate reduced elastic modulus E_r and hardness H_{nano} versus indentation depth h by the Oliver and Pharr method. It can be seen that, for all samples and all indents, H_{nano} decreases with h (Fig. 4e and Fig. A2) due to the indentation size effect (ISE), which is usually observed in metallic alloys [27], including high entropy alloys [28]To have a limited and similar ISE for all samples, E_r and H_{nano} were averaged for indentation depth between 350 and 400 nm (as indicated by the black arrow on Fig. 4d and e). They were also averaged on the one hundred indents performed on each sample. The averaged values are named $\overline{\boldsymbol{E}}_{\boldsymbol{nano}}$ and $\overline{\boldsymbol{H}}_{\boldsymbol{nano}}$**.** The given uncertainty corresponds to the standard deviation on the averaged values. The reduced elastic modulus E_r has to be converted into the Young modulus E_{nano} [29]. Poisson's ratio of 0.304 and 0.265, which were measured on pure Ni and CoCrFeMnNi HEA [30], were used for Ni92-A and Ni20-A respectively. For Ni60-A samples, not knowing the Poisson ratio's, an average value of the ratios of Ni and CoCrFeMnNi (i.e.: 0.284) was used. The nanoindentation procedure is detailed in [31].

Table 1 : List of the studied samples and of their measured microstructural and mechanical properties

Sample name	Composition (% at.)	Recristallization	Grain size (µm)	E (GPa)	YS (MPa)	UTS (MPa)	ε_r
Ni20-rec1	$Co_{20}Cr_{20}Fe_{20}Mn_{20}Ni_{20}$	900°C, 1h	13 ± 1	214 ± 18	318 ± 2	631 ±7	0.37 ± 0.009
Ni60-rec1	$Co_{10}Cr_{10}Fe_{10}Mn_{10}Ni_{60}$	800°C, 2h	12 ± 1	219 ± 16	308 ± 7	642 ± 3	0.35 ± 0.006
Ni92-rec1	$Co_2Cr_2Fe_2Mn_2Ni_{92}$	800°C, 8h	14 ± 1	181 ± 8	183 ± 1	446 ± 3	0.38 ± 0.005
Sample name	**Composition (% at.)**	**Recristallization**	**Grain size (µm)**	$\overline{E}_{nano}$ **(GPa)**	$\overline{H}_{nano}$ **(GPa)**		
Ni20-homog	$Co_{20}Cr_{20}Fe_{20}Mn_{20}Ni_{20}$	-*	≥ 200	203 ± 10	2.5 ± 0.07		
Ni60-homog	$Co_{10}Cr_{10}Fe_{10}Mn_{10}Ni_{60}$	-*	≥ 200	226 ± 7	2.94 ± 0.08		
Ni92-homog	$Co_2Cr_2Fe_2Mn_2Ni_{92}$	-*	≥ 200	211 ± 10	1.99 ± 0.06		
Ni20-rec2	$Co_{20}Cr_{20}Fe_{20}Mn_{20}Ni_{20}$	1250°C, 3h	440 ± 40	193 ± 9	2.68 ± 0.01		
Ni60-rec2	$Co_{10}Cr_{10}Fe_{10}Mn_{10}Ni_{60}$	1250°C, 3h	430 ± 80	189 ± 17	2.88 ± 0.05		
Ni92-rec2	$Co_2Cr_2Fe_2Mn_2Ni_{92}$	1250°C, 3h	730 ± 40	205 ± 8	1.93 ± 0.05		

Recrystallization: temperature and duration of the recrystallization annealing

E, YS, UTS and ε_r: Young modulus, yield strength, engineering ultimate tensile stress and engineering strain at rupture respectively, measured by tensile tests

E_{nano}, H_{nano}: Young modulus and nanohardness respectively, measured by nanoindentation

** no recrystallization annealing for those samples*

3. Results and discussion

3.1. Tensile tests

Recrystallized specimen are required for tensile tests. To preferentially assess the solid solution strengthening (SSS) and its evolution with composition, it was chosen to have a similar grain size of around 15 µm for the three compositions. This value is a compromise between maximizing grain size to minimize the grain boundary strengthening and keeping a sufficiently high number of grains in the specimen. In a first approximation, the grain boundary strengthening can be considered limited and equivalent for the three compositions.

It is recalled that the three studied compositions were previously characterized as single-phase face centered cubic (fcc) solid solutions [21, 32]. The grains of the recrystallized samples are depicted in Fig. 1. The uniform distribution of grain size indicates that the three samples are fully recrystallized. Moreover, according to Fig. 1b, Ni20-rec1 and Ni-60rec1 have isotropic grains while Ni92-rec1 exhibits a preferential <101> orientation. Finally, as can be seen on Fig. 1a, Ni20-rec1 contains more annealing twins (i.e.: Σ3 boundaries, which are plotted in red) than Ni60-rec1 and Ni92-rec1. From those images, an average grain size of 13, 12 and 14 µm was determined for Ni20-rec1, Ni60rec1 and Ni92-rec1 respectively (Table 1). It is underlined that, to obtain

these very similar grain sizes, different recrystallization conditions were used. This is illustrative of the fact that grain growth kinetic significantly varies with composition.

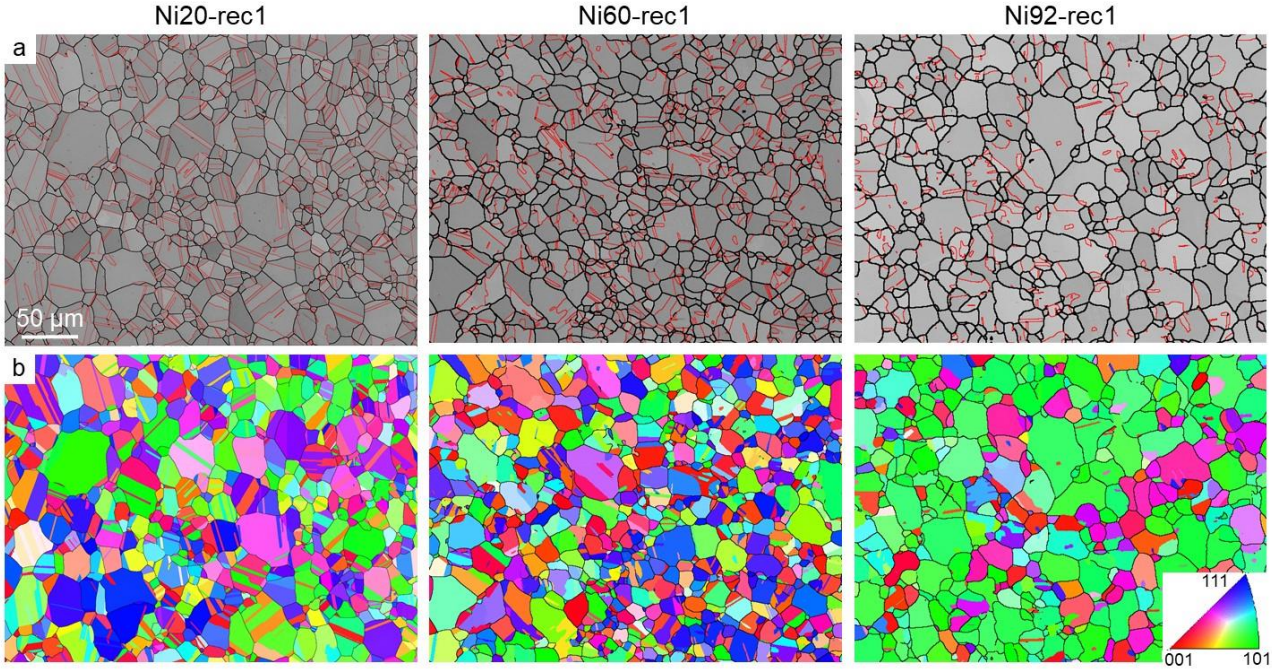

Fig. 1 : Electron BackScattered Diffraction (EBSD) mapping of the three alloys after recrystallization annealing at a medium temperature. (a) Grain boundary disorientation map superimposed on the band contrast map. Lines are in black for high angle boundaries ($5 < \vartheta < 58°$ and $\vartheta > 62°$) and in red for Σ3 boundaries ($\vartheta = 60° \pm 2$), with ϑ the disorientation angle. (b) Orientation map superimposed with grain boundary disorientation map (black lines for $5 < \vartheta < 58°$ and $\vartheta > 62°$). The standard stereographic triangle is in the right down corner. The scale is the same for all six images.

On Fig. 2a and b, it can be seen that Ni20-rec1 and Ni60-rec1 tensile curves are nearly superimposed. Indeed, Ni20-rec1 and Ni60-rec1 have equivalent yield strength (YS) of respectively 318 ± 2 and 308 ± 7 MPa and ultimate tensile strength (UTS) of respectively of 631 ± 7 and 642 ± 3 MPa. The mechanical properties of Ni20-rec1 are in good quantitative agreement with previous studies on the Cantor alloy with a similar grain size [11, 33]. Moreover, it can be seen that Ni92-rec1 has a lower stress than Ni20-rec1 and Ni60-rec1 for any strain. Indeed, the YS and UTS of Ni92-rec1 are respectively 183 ± 1 and 446 ± 3 MPa. Thus, the YS and UTS increase respectively of 135 MPa (74 %) and 185 MPa (42 %) between Ni92-rec1 on the one hand and Ni20-rec1 and Ni60-rec1 on the other hand. As a comparison, the yield stress of pure Ni with an equivalent grain size of 18 µm was measured to be 32 MPa [34], which corresponds to an increase of 151 MPa (470 %) between pure Ni and Ni92-rec1. This is more significant than the increase between Ni92-rec1 and Ni60-rec1. Besides, all samples have an elongation at rupture larger than 35 %, which means that the three alloys are equivalently very ductile. As expected from the large difference between YS and UTS and as usually observed for fcc crystalline structure [35], the strain hardening is high for the three Nix-rec1 samples (Fig. 2c). More precisely, the strain hardening of Ni92-rec1 is lower than the ones of Ni20-rec1 and Ni60-rec1, especially between 0.1 and 0.3 of plastic strain. Thus, the concentrated fcc solid solution influences not only the onset of plasticity but also the strain hardening. It is mentioned that, on the contrary, concentrated body centered cubic solid solutions exhibit a limited strain hardening [36]. It can also be noticed that the strain hardening of Ni60-rec1 is slightly larger than the one of Ni20-rec1 between 0.1 and 0.25 of plastic strain. This might be due to an additional deformation mechanism, like nanotwinning which was observed in the Cantor alloy at cryogenic temperature [11] and in CoCrNi at room temperature [15], at the same strain rate loading than in this study. An evolution of the stacking fault energy with the composition, which has already been shown for equimolar alloys of the Co-Cr-Fe-Mn-Ni system [37], is another possible explanation.

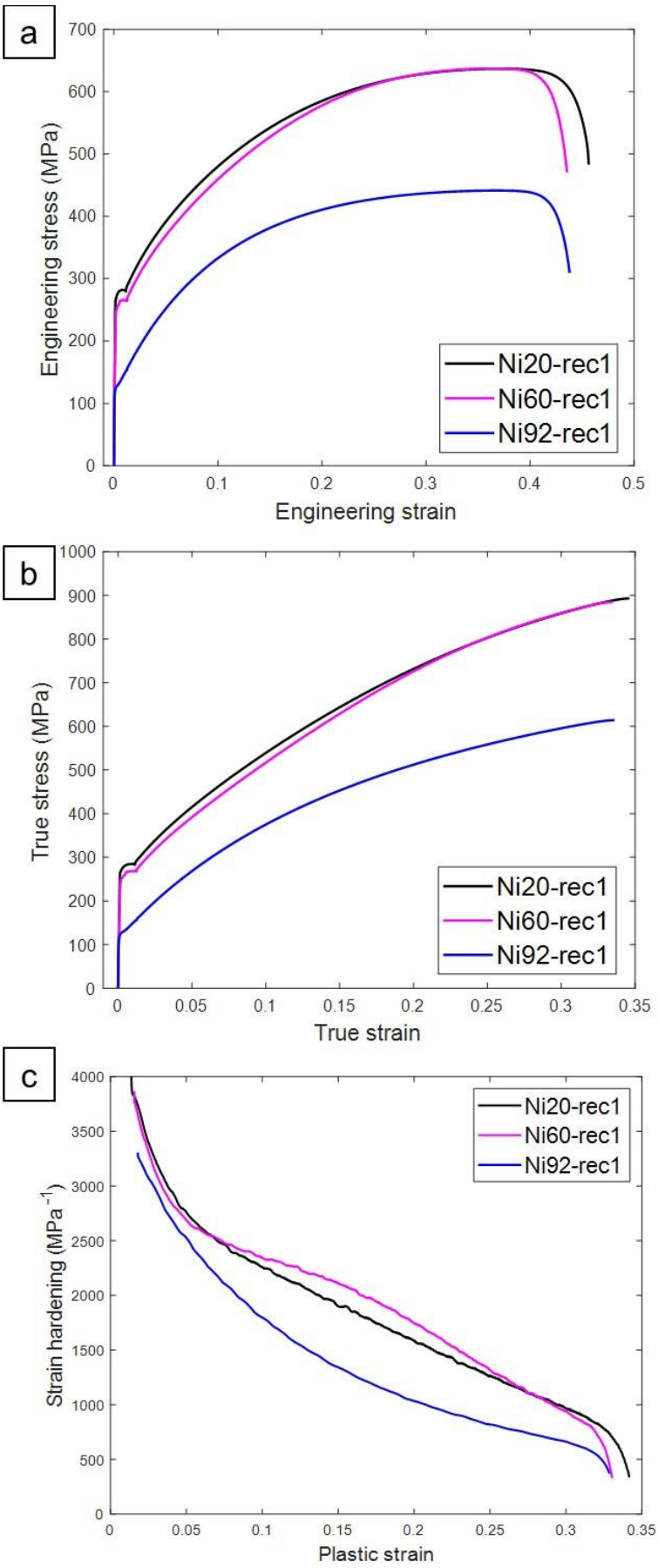

Fig. 2 : Tensile tests on the three recrystallized alloys. (a) Engineering stress-strain curves. (b) True stress-strain curves. (c) Strain hardening $d\sigma_T/d\varepsilon_p$ as a function of plastic strain with σ_T the true stress and ε_p the plastic strain.

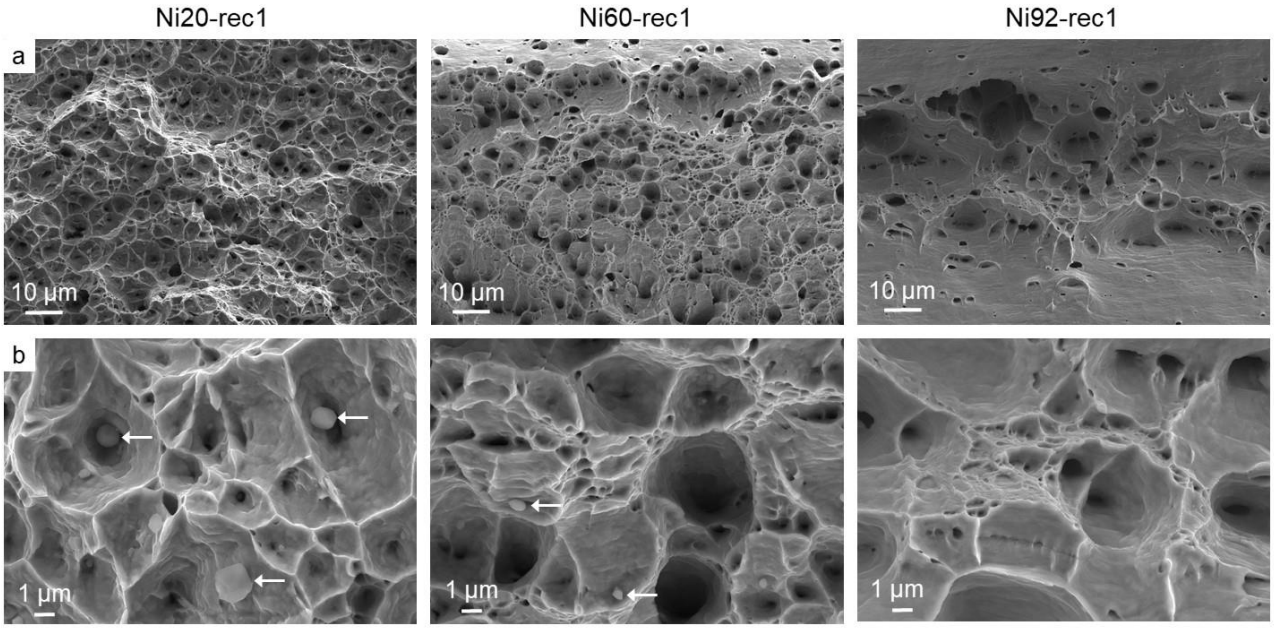

Fig. 3 : Scanning electron microscope images of the fractured recrystallized samples after tensile tests. A Secondary Electron (SE) dectector was used. White arrows indicate precipitates.

The characterization of the three Nix-rec1 alloys after tensile tests confirm their very ductile nature. Indeed, dimples, which are indicative of microvoid coalescence, can be observed on the three fractured surfaces (Fig. 3). The dimples in Ni20-rec1 and Ni60-rec1 have similar dimensions, which range from 2 to 7 µm. Ni92-rec1 exhibits slightly larger dimples, up to around 20 µm. It is mentioned that the necking of Ni92-rec1 was more pronounced than for the two other compositions. Micronic and submicronic precipitates, which act as initiation sites for voids, can be observed inside the dimples of Ni20-rec1 and Ni60-rec1 (Fig. 3b). Their diameter varies between 0.3 and 2 µm for Ni20-rec1 and 0.3 and 0.5 µm for Ni60-rec1. So the size is slightly larger for Ni20-rec1. Their density also seems to be larger. According to EDS analysis, these precipitates are enriched in Mn and O and sometimes also contain Al or S, which are very likely impurities from raw metals. For Ni92-rec1, there are seldom precipitates, which are always smaller than 0.5 µm. First, it can be concluded that the three fcc solid solutions guarantee a very high ductility, even in the presence of micronic precipitates. Second, the size and density of the precipitates seems qualitatively correlated with the composition: they decrease when the content of Ni increases. This is likely due to the fact that the content of Mn, which is the main element of the precipitates, decreases when Ni increases.

To summarize, increasing the solute content compared to conventional diluted solid solutions is a very efficient way to increase not only the YS but also the UTS and the strain hardening without reducing the ductility. It has to be underlined that it is unnecessary to reach an equimolar content of elements to maximize this effect. Indeed, the alloy $(CoCrFeMn)_{40}Ni_{60}$ exhibits as high mechanical properties as the well-known equimolar Cantor alloy. It has also to be highlighted that the SSS is not accentuated when the composition goes from diluted solid solution towards medium and high entropy alloys. Indeed, the increase of yield strength is more significant between pure Ni and $(CoCrFeMn)_8Ni_{92}$ than between $(CoCrFeMn)_8Ni_{92}$ and $(CoCrFeMn)_{40}Ni_{60}$.

3.2. Nanoindentation

The following nanoindentation procedure was used: ten positions were randomly chosen on a sample and at each position, a group of ten indents was performed. This large number of one hundred indents per sample is intended to provide a reliable averaging of properties, despite the local nature of nanoindentation. Next, given the width of indent print of around 3 µm, the size of group of ten indents of 10*40 µm² and the length

of grain of more than 200 µm² (Table 1), this specific procedure induces that one group of indents, is very likely to be within a grain, far away from grain boundaries. The first consequence is that grain boundary effect on hardness measurements can be neglected, which is an advantage for this study whose main interest is SSS. The second consequence is that various crystalline orientations are tested. More precisely, one position is very likely to be placed on the same orientation while different positions are likely to correspond to different orientations (Fig. 4b). It was observed that the variation of crystalline orientation has on impact on elastic modulus. On Fig. 4d, the elastic modulus of the thirty indents of 3 positions are plotted. It can be observed that the curves of the indents from a same position are very close while there is a significant difference between positions. This reflects an anisotropy of elastic constants, which was indeed calculated by ab-initio for the Cantor alloy [38]. The issue is that the values obtained on the ten positions are not sufficient to average the effect of anisotropy. This is why there is, for example, a difference of 37 GPa between E_{nano} of Ni60-homog and Ni60-rec2, which is significantly larger than the uncertainty. It also explains the difference of 30 GPa between E_{nano} for Ni92-homog and the Young modulus measured by tensile test for Ni92-rec1. Thus, the measured E_{nano} were not further analyzed. On the contrary, it should be underlined that the crystalline orientation has no significant influence on hardness. Indeed, on Fig. 4e, for the indents of the same three positions which were sensitive to orientation for E_{nano}, the curves of H_{nano} overlap.

The nanohardness of the three studied composition was measured on two types of samples: (i) the Nix-homog samples and (ii) the Nix-rec2. The interest of the first ones is that they were produced by the accelerated processing route (i.e.: only melting, casting and homogeneization). As a result, grains are large, with various dimension and with irregular shape (Fig. A1a). The interest of the second ones is that, since they were recrystallized, they should have a closer metallurgical state compared to the Nix-rec1 samples, which were tested by tensile test, than the homogenized samples. It is underlined that a large grain size was preferred, contrary to the tensile test specimen, in order to avoid the influence of grain boundaries (Fig. A1b). A nanohardness of 2.5 ± 0.07, 2.94 ± 0.08 and 1.99 ± 0.06 GPa was measured respectively for Ni20-homog, Ni60-homog and Ni92-homog. The nanohardness increases respectively of 26 % and 48 % between Ni92-homog on the one hand and Ni20-homog and Ni60-homog on the other hand. It should be noticed that those percentage of increase are significantly different than the ones observed for YS. Finally, the nanohardness of Nix-homog and Nix-rec2 samples, for a given composition, exhibit some differences which are either slightly larger or of the same order of magnitude than the uncertainty. The comparison between the hardness on different samples and the yield strength is further discussed in the following sub-section.

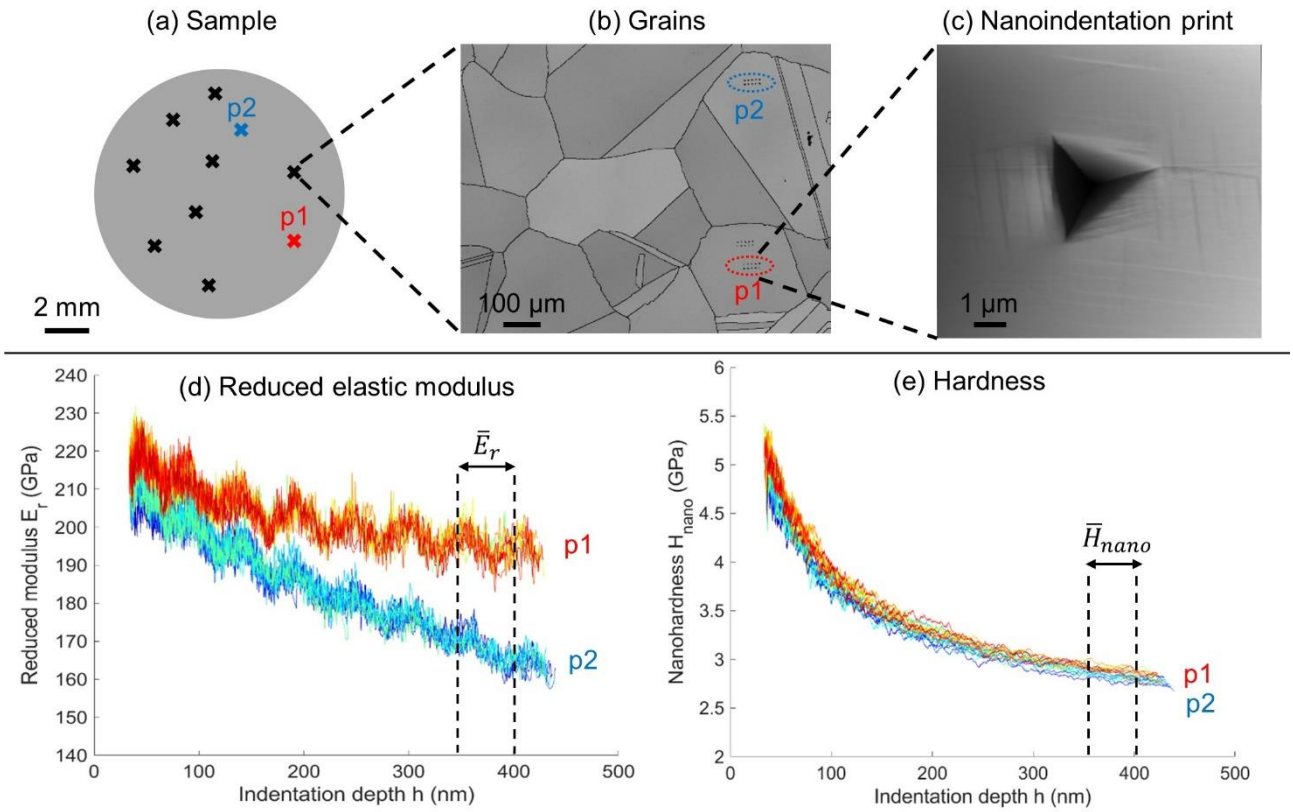

Fig. 4 : Presentation of nanoindentation measurements. (a) Scheme of the shape of the alloys and of the randomly distributed positions which were tested (black and colored cross). (b) EBSD mapping of one sample (band contrast and grain boundaries). Two groups of ten indents, which correspond to p1 and p2, are circled. (c) Topography image of a nanoindentation indent obtained by SPM. (d) Evolution of the reduced Young modulus E_r with indentation depth h measured for the groups p1 and p2 from Ni60-rec2. (e) Evolution of nanohardness H_{nano} with indentation depth h. The same colors as in (d) are attributed for each indent. The range of averaging of $H_{nano}(h)$ and $E_{nano}(h)$ are indicated with a black arrow.

3.3. Comparison between tensile tests and nanoindentation

Broadly speaking, converting hardness into yield strength is not straightforward. Indeed, a uniaxial stress is applied during tensile test whereas a complex stress field, which depends on the tip geometry, is created by indentation. Moreover, indentation induces a plastic strain, of 7 % for a Berkovich tip [29], whereas the yield strength is determined at the onset of plasticity, usually at only 0.2 % of plastic deformation. Several models exist, which can be either simple like the Tabor's equation [39] or more complex like the model of Clausner *et al.* [40], which requires to know the strain hardening coefficient. Nevertheless, the accuracy of those models depends on the type of materials and on the choice of the parameters, when needed. Nanoindentation has been widely used on high entropy as reported in the review of Zou *et al.* on nanomechanical studies of HEA [41]. In some cases, nanohardness is only qualitatively compared with yield strength [20, 23] or is converted into a yield strength through the simple Tabor's equation [21, 22]. Lee *et al.* [42] quantitatively converted H of the Cantor alloy into a yield strength with an approach close to the Clausner *et al.* model with an additional assumption of a negligible strain hardening effect. They obtain only a qualitative agreement with tensile results. For four HEA of the Co-Cr-Fe-Mn-Ni systems, Coury *et al.* [19] convert H into a yield strength using the Tabor's equation, the Clausner model with or without assumption of a negligible strain hardening and they did not obtain a quantitative agreement in any case when comparing with experimental yield strength. Alternatively, they fit the parameters of the Clausner model on experimental yield strengths. Since those parameters have not been applied yet for compositions which were not used for fitting, the robustness of this approach can not be assessed. These studies illustrate the fact that

using nanohardness to quantitatively determine the yield strength remains challenging for HEA, which limits the use of nanoindentation as a tool for fast exploring of chemical compositions.

In this context, a quantitatively comparative and experimental approach, dedicated to single-phase HEA, was preferred. In other words, it was chosen to quantitatively compare the evolution with the composition of the mechanical properties. To do so, the composition Ni20 was set as the reference and the ratio X(60Ni)/X(20Ni) and X(92Ni)/X(20Ni), where X is a mechanical data which describes the mechanical strength, were calculated. X can be the yield strength and the stress at 7 % of plastic deformation, which were determined by tensile test on Nix-rec1 samples. X is also the nanohardness of homogenized samples (Nix-homog) and recrystallized samples with large grains (Nix-rec2), which was measured by nanoindentation. As can be seen on Fig. 5, the same general tendencies are observed for the four type of ratios: (i) the mechanical strength of Ni92 is smaller than the one of both Ni60 and Ni20, (ii) the mechanical strength of Ni60 is close from the one of Ni20. Quantitatively, the ratios of stress at 7 % of plastic deformation and the nanohardness of recrystallized samples are equal, providing the experimental uncertainty. It proves that nanoindentation and tensile tests can be reliably and quantitatively compared. Nevertheless, there is around 20 % of difference between the ratios of yield strength and of nanohardness on homogenized samples for both compositions. This can be explained by two reasons. First, since the strain hardening depends on the composition, nanohardness is more precisely compared with tensile data corresponding to the same deformation state (i.e.: stress at 7 % of plastic deformation). This point impacts mainly Ni92 and is less significant for Ni60, whose strain hardening is nearly equal to the one of Ni20, at least up to 7 % of plastic deformation. Second, the difference between the nanohardness of Nix-homog and Nix-rec2 samples is very likely reflective of an evolution of the density of pre-existing dislocations, which seems to slightly depend on the composition. Combining these two effects leads to an uncertainty of 20 % when assessing the yield strength of HEA by nanoindentation on homogenized samples.

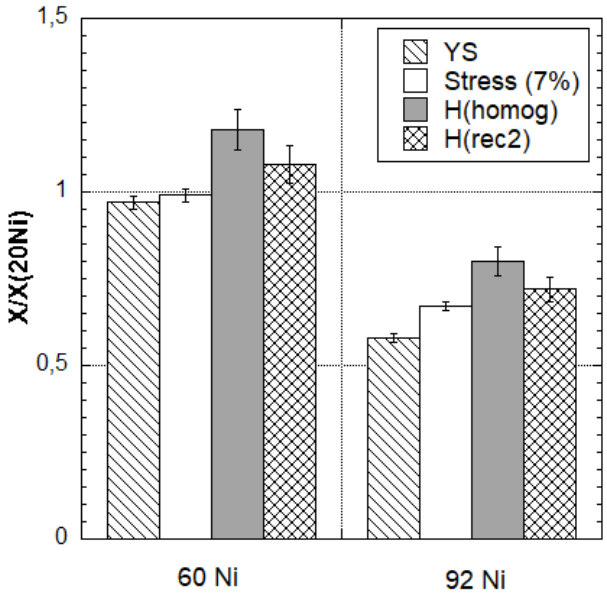

Fig. 5 : Comparison between tensile tests and nanoindentation measurements. Ratios X(60Ni)/X(20Ni) and X(92Ni)/X(20Ni). X is the yield strength (YS) and the engineering stress at 7% of plastic strain (Stress(7%)) which were measured by tensile tests on recrystallized samples. X is also the nanohardness measured by nanoindentation on homogenized samples (H(homog)) and on recrystallized samples (H(rec2)).

Thus, nanoindentation is a significantly less precise method than tensile tests to determine the yield strength. Nonetheless, nanoindendation allowsfast mechanical testing compared to tensile tests because the preparation of sample is significantly easier and faster. Indeed, since nanoindentation is a local technique, it is appropriate for small size sample. Thus the conventional metallurgical multi-step process (melting, casting,

homogeneization annealing, cold-rolling, recrystallization annealing and sample machining, as in [43]) was reduced to the first three steps. Not only it shortens the time to produce one sample, but it also drastically reduces the need for condition optimization since, as it was seen in this study, the parameters for recrystallization significantly depend on the composition, contrary to the first three steps of processing. A second advantage of nanoindentation is that it allows to study exclusively the solid solution strengthening. In [16, 44, 45], where tensile tests were performed, a possible influence of small grain size variations or of oxides on yield strength could not be excluded. To conclude, nanoindentation on homogenized samples is a powerful tool to explore the solid solution strengthening of a wide range of compositions and then to identify the most promising ones. In a second step, complete metallurgical processing and tensile testing on a limited number of pre-selected compositions permit to confirm the SSS and to measure other mechanical properties, as strain hardening or ductility.

4. Conclusion

Three single-phase alloys from the quinary Co-Cr-Fe-Mn-Ni system were studied: (i) the equimolar CoCrFeMnNi HEA, (ii) the $(CoCrFeMn)_{40}Ni_{60}$ MEA and (iii) the conventional $(CoCrFeMn)_2Ni_{92}$ alloy. Each of them was processed into three metallurgical states: homogenized, recrystallized with grains of around 15 µm and recrystallized with large grains. Their microstructure was characterized by scanning electron microscopy coupled with Electron BackScattered Diffraction and their mechanical properties were measured by tensile tests and nanoindentation. The main conclusions are the following:

- The $(CoCrFeMn)_{40}Ni_{60}$ MEA, with an average grain size of 12 µm, exhibits a yield strength (YS), an ultimate tensile strength (UTS) and an elongation at rupture of 308 MPa, 642 MPa and 0.35 respectively. These properties are as good as the well-known equimolar CoCrFeMnNi HEA.
- The YS and UTS increase respectively of 74 % and 42 % between the conventional $(CoCrFeMn)_2Ni_{92}$ alloy on the one hand and the $(CoCrFeMn)_{40}Ni_{60}$ MEA and CoCrFeMnNi HEA on the other hand.
- The fracture of the three alloys is ductile. The fractured surfaces are composed of dimples which contain precipitates, mainly manganese oxides.
- More broadly speaking, increasing the solute content compared to conventional diluted solid solutions induces a large increase of the mechanical strength without reducing the ductility. Still, it is unnecessary to reach an equimolar content of elements to maximize the solid solution strengthening (SSS).
- Hardness measured by nanoindentation on homogenized samples and yield strength measured by tensile tests on recrystallized samples are comparable with a maximum uncertainty of 20 % for the studied compositions.
- Measuring hardness by nanoindentation on small size and only homogenized samples is a powerful strategy to explore the SSS of the wide space of compositions of HEA. Combining these measurements with tensile tests on the most promising compositions is necessary to fully assess the mechanical properties.

In the future, this strategy will be applied to fully explore the Co-Cr-Fe-Mn-Ni system.

5. Acknowledgements

The authors are grateful to J.-P. Couzinié from ICMPE for fruitful discussions.

6. Appendices

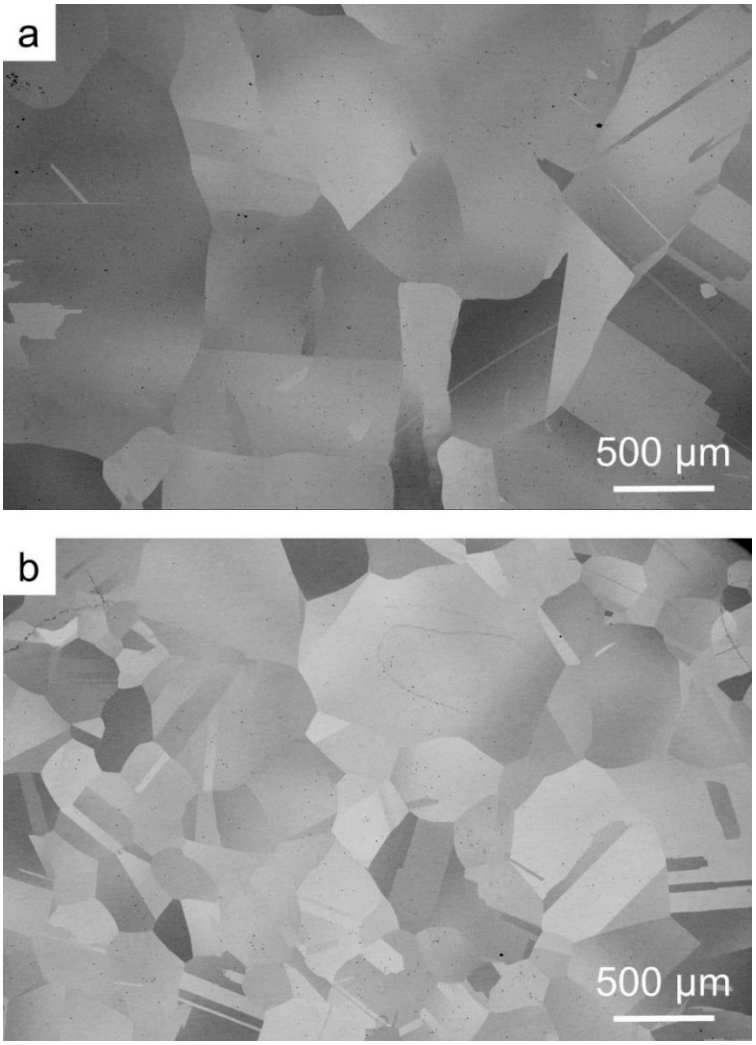

Fig. A1 : Scanning electron microscope images of (a) Ni60-homog and (b) Ni60-rec2.

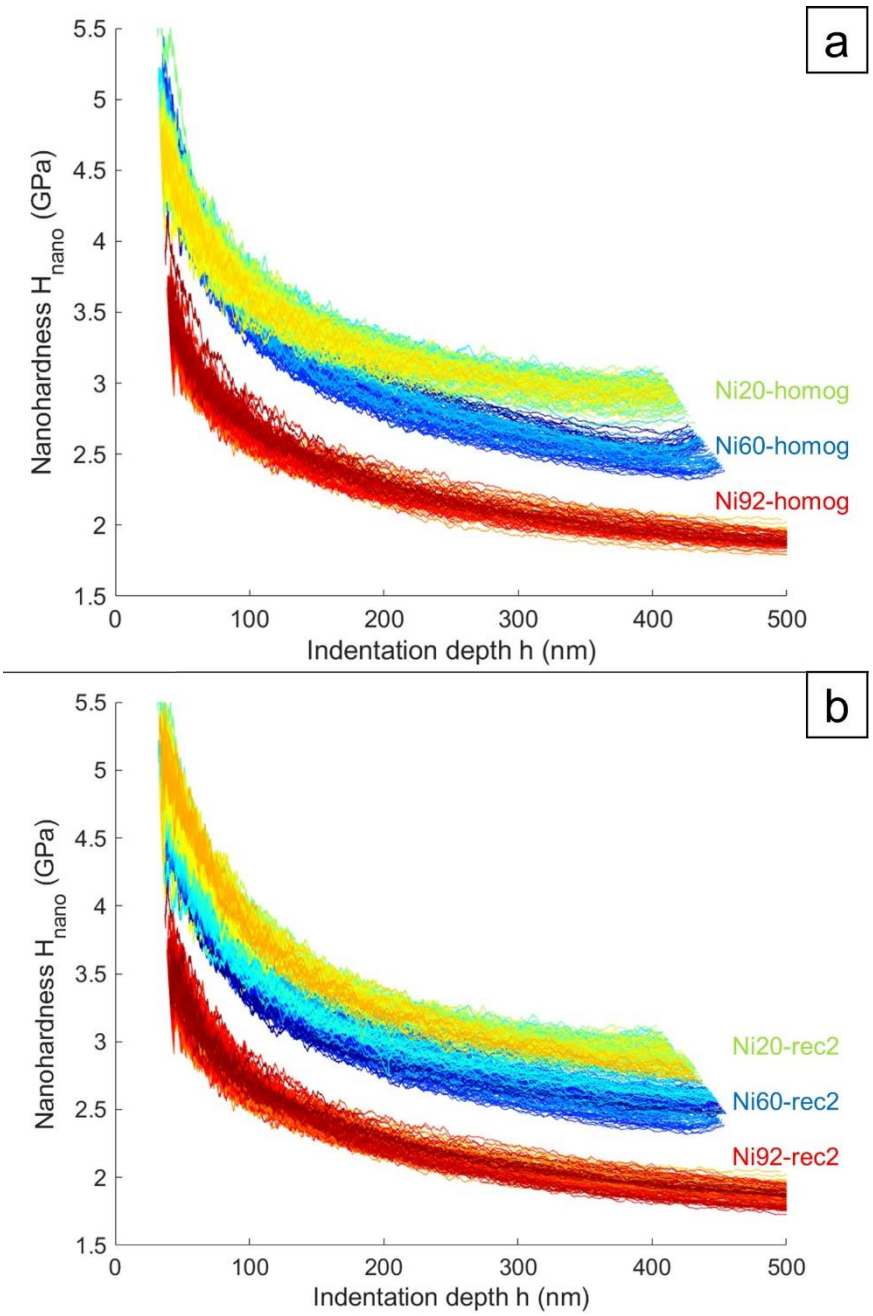

Fig. A2 : Evolution of nanohardness H_{nano} with indentation depth h for (a) the three homogenized samples(Nix-homog) and for (b) the three recrystallized samples (Nix-rec2). For each sample, one hundred curves, which correspond to all the indents randomly distributed on the samples, are plotted with varying colors.

Table A1 : Average composition of the studied samples, which was measured by SEM-EDS mapping.

	Measured composition (at. %)				
Sample name	Co	Cr	Fe	Mn	Ni
Ni20-rec1	20.0	20.3	19.9	20.1	19.7
Ni60-rec1	10.1	10.3	10.2	10.3	59.1
Ni92-rec1	2.1	2.1	2.1	2.2	91.5

Ni20-homog	19.9	20.1	19.7	20.4	19.9
Ni60-homog	10.4	10.5	10.4	9.6	59.1
Ni92-homog	2.2	2.1	2.2	2.3	91.2
Ni20-rec2	19.9	20.3	19.8	20.2	19.8
Ni60-rec2	10.1	10.3	10.1	10.4	59.1
Ni92-rec2	2.1	2.1	2.2	2.3	91.3

7. References

[1] Yeh, J.W., S.K. Chen, S.J. Lin, J.Y. Gan, T.S. Chin, T.T. Shun, C.H. Tsau, and S.Y. Chang, *Advanced Engineering Materials*, 6, 299-303 (2004).

[2] Cantor, B., I.T.H. Chang, P. Knight, and A.J.B. Vincent, *Materials Science and Engineering: A*, 375–377, 213-218 (2004).

[3] Miracle, D.B. and O.N. Senkov, *Acta Materialia*, 122, 448-511 (2017).

[4] Pickering, E.J. and N.G. Jones, *International Materials Reviews*, 61, 183-202 (2016).

[5] Ye, Y.F., Q. Wang, J. Lu, C.T. Liu, and Y. Yang, *Materials Today*, 19, 349-362 (2016).

[6] Yeh, J.-W., *JOM*, 67, 2254-2261 (2015).

[7] Gorsse, S., J.-P. Couzinié, and D.B. Miracle, *Comptes Rendus Physique*, 19, 721-736 (2018).

[8] Laurent-Brocq, M., A. Akhatova, L. Perrière, S. Chebini, X. Sauvage, E. Leroy, and Y. Champion, *Acta Materialia*, 88, 355-365 (2015).

[9] Otto, F., A. Dlouhý, C. Somsen, H. Bei, G. Eggeler, and E.P. George, *Acta Materialia*, 61, 5743-5755 (2013).

[10] Gludovatz, B., A. Hohenwarter, D. Catoor, E.H. Chang, E.P. George, and R.O. Ritchie, *Science*, 345, 1153-1158 (2014).

[11] Laplanche, G., A. Kostka, O.M. Horst, G. Eggeler, and E.P. George, *Acta Materialia*, 118, 152-163 (2016).

[12] Senkov, O.N., J.D. Miller, D.B. Miracle, and C. Woodward, *Nature Communication*, 6, (2015).

[13] Bracq, G., M. Laurent-Brocq, L. Perrière, R. Pirès, J.-M. Joubert, and I. Guillot, *Acta Materialia*, 128, 327-336 (2017).

[14] Gludovatz, B., A. Hohenwarter, K.V.S. Thurston, H. Bei, Z. Wu, E.P. George, and R.O. Ritchie, *Nature Communication*, 7, (2016).

[15] Laplanche, G., A. Kostka, C. Reinhart, J. Hunfeld, G. Eggeler, and E.P. George, *Acta Materialia*, 128, 292-303 (2017).

[16] Stepanov, N.D., D.G. Shaysultanov, M.A. Tikhonovsky, and G.A. Salishchev, *Materials & Design*, 87, 60-65 (2015).

[17] Pradeep, K.G., C.C. Tasan, M.J. Yao, Y. Deng, H. Springer, and D. Raabe, *Materials Science and Engineering: A*, 648, 183-192 (2015).

[18] Wu, Z., H. Bei, G.M. Pharr, and E.P. George, *Acta Materialia*, 81, 428-441 (2014).

[19] Coury, F.G., P. Wilson, K.D. Clarke, M.J. Kaufman, and A.J. Clarke, *Acta Materialia*, 167, 1-11 (2019).

[20] Wilson, P., R. Field, and M. Kaufman, *Intermetallics*, 75, 15-24 (2016).

[21] Laurent-Brocq, M., L. Perrière, R. Pirès, F. Prima, P. Vermaut, and Y. Champion, *Materials Science and Engineering: A*, 696, 228-235 (2017).

[22] Jin, K., Y.F. Gao, and H. Bei, *Materials Science and Engineering: A*, 695, 74-79 (2017).

[23] Chen, H., A. Kauffmann, S. Laube, I.C. Choi, R. Schwaiger, Y. Huang, K. Lichtenberg, F. Muller, B. Gorr, H.J. Christ, and M. Heilmaier, *Metallurgical and Materials Transactions a-Physical Metallurgy and Materials Science*, 49A, 772-781 (2018).

[24] Wu, Z., H. Bei, F. Otto, G.M. Pharr, and E.P. George, *Intermetallics*, 46, 131-140 (2014).

[25] *ASTM International*, E112-12, (2012).

[26] Laurent-Brocq, M., E. Béjanin, and Y. Champion, *Scanning*, 9999, 1-11 (2015).

[27] Nix, W.D. and H. Gao, *Journal of the Mechanics and Physics of Solids*, 46, 411-425 (1998).

[28] Maier-Kiener, V., B. Schuh, E.P. George, H. Clemens, and A. Hohenwarter, *Materials & Design*, 115, 479-485 (2017).

[29] Fischer-Cripps, A.C., *Nanoindentation* (New York, Springer, 2011), pp.

[30] Haglund, A., M. Koehler, D. Catoor, E.P. George, and V. Keppens, *Intermetallics*, 58, 62-64 (2015).

[31] Bracq, G., M. Laurent-Brocq, C. Varvenne, L. Perrière, W.A. Curtin, J.-M. Joubert, and I. Guillot, *Acta Materialia*, doi.org/10.1016/j.actamat.2019.06.050.

[32] Laurent-Brocq, M., L. Perrière, R. Pirès, and Y. Champion, *Materials & Design*, 103, 84-89 (2016).

[33] Sun, S.J., Y.Z. Tian, H.R. Lin, X.G. Dong, Y.H. Wang, Z.J. Zhang, and Z.F. Zhang, *Materials & Design*, 133, 122-127 (2017).

[34] Feaugas, X. and H.J.M. Haddou, *Metallurgical Materials Transactions A*, 34, 2329-2340 (2003).

[35] Kocks, U.F. and H. Mecking, *Progress in Materials Science*, 48, 171-273 (2003).

[36] Lilensten, L., J.P. Couzinié, L. Perrière, A. Hocini, C. Keller, G. Dirras, and I. Guillot, *Acta Materialia*, 142, 131-141 (2018).

[37] Zaddach, A.J., C. Niu, C.C. Koch, and D.L. Irving, *JOM*, 65, 1780-1789 (2013).

[38] Zhang, H., X. Sun, S. Lu, Z. Dong, X. Ding, Y. Wang, and L. Vitos, *Acta Materialia*, 155, 12-22 (2018).

[39] Tabor, D., *Hardness of metals* (Oxford, Clarendon Press, 1951), pp.

[40] Clausner, A. and F. Richter, *European Journal of Mechanics - A/Solids*, 51, 11-20 (2015).

[41] Zou, Y., *Journal of Materials Research*, 33, 3035-3054 (2018).

[42] Lee, D.-H., J.-A. Lee, Y. Zhao, Z. Lu, J.-Y. Suh, J.-Y. Kim, U. Ramamurty, M. Kawasaki, T.G. Langdon, and J.-i. Jang, *Acta Materialia*, 140, 443-451 (2017).

[43] Otto, F., N.L. Hanold, and E.P. George, *Intermetallics*, 54, 39-48 (2014).

[44] Deng, Y., C.C. Tasan, K.G. Pradeep, H. Springer, A. Kostka, and D. Raabe, *Acta Materialia*, 94, 124-133 (2015).

[45] Zaddach, A.J., R.O. Scattergood, and C.C. Koch, *Materials Science and Engineering: A*, 636, 373-378 (2015).

Tensile tests

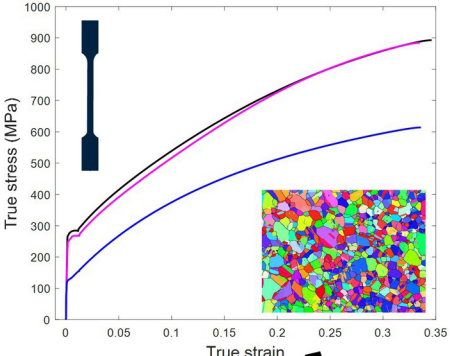

Comparison

Nanoindentation

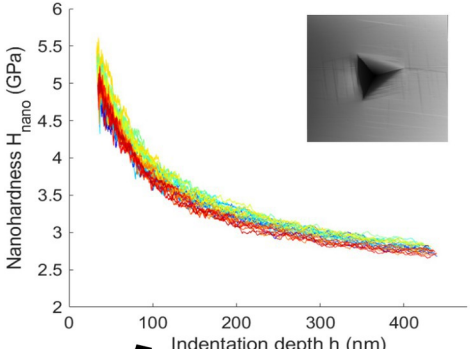

New medium entropy alloy

$(CoCrFeMn)_{40}Ni_{60}$